A Biologically Inspired Hair Aging Model

ARTHUR E. BALBÃO and MARCELO WALTER, UFRGS - Institute of Informatics, Brazil

Fig. 1. Hair Aging simulation from our system. From left to right, increasing the hair aging for the same virtual character. From top to bottom: white male, white female with reddish hair, and black male with facial hair.

Hair rendering has been a focal point of attention in computer graphics for the last couple of decades. However, there have been few contributions to the modeling and rendering of the natural hair aging phenomenon. We present a new technique that simulates the process of hair graying and hair thinning on digital models due to aging. Given a 3D human head model with hair, we first compute a segmentation of the head using K-means since hair aging occurs at different rates in distinct head parts. Hair graying is simulated according to recent biological knowledge on aging factors for hairs, and hair thinning decreases hair diameters linearly with time. Our system is biologically inspired, supports facial hair, both genders and many ethnicities, and is compatible with different lengths of hair strands. Our real-time results resemble real-life hair aging, accomplished by simulating the stochastic nature of the process and the gradual decrease of melanin.

CCS Concepts: • **Computing methodologies** → **Computer graphics**; **Rendering**;

Additional Key Words and Phrases: computer graphics, hair rendering, hair aging

ACM Reference Format:
Arthur E. Balbão and Marcelo Walter. 2022. A Biologically Inspired Hair Aging Model. *ACM Trans. Graph.* 41, 6, Article 223 (December 2022), 9 pages. https://doi.org/10.1145/3550454.3555444

Authors' address: Arthur E. Balbão, arthur.balbao@inf.ufrgs.br; Marcelo Walter, marcelo.walter@inf.ufrgs.br, UFRGS - Institute of Informatics, Porto Alegre, RS, Brazil.

0730-0301/2022/12-ART223 $15.00
https://doi.org/10.1145/3550454.3555444

1 INTRODUCTION

The accurate digital representation of humans and our intricate details has long attracted the interest of computer graphics research. From early efforts [Ko et al. 2003; Magnenat-Thalmann 2004; Ryder and Day 2005] to state-of-the-art representations [Gitlina et al. 2020; Iglesias-Guitian et al. 2015; Lombardi et al. 2021], we already have results that are being used in many applications. One of the most challenging elements to represent in a digital human is the hair scalp due to the number of primitives, geometric complexity, and the associated light interactions, such as subsurface scattering and

self-shadowing. Although many advancements in shading [Chiang et al. 2016; Zinke et al. 2008] and the polygonal representation of hair [Jansson et al. 2019; Petrovic et al. 2005], hair aging in digital assets is currently not addressed.

We use from Biology the concept of aging factor for hairs [Rosenberg et al. 2021] and present a method for realistic simulation of hair aging in digital humans. Our main contribution is a model for hair graying and thinning that is biologically inspired, runs in real-time, and adapts to any hairstyle and facial hair.

2 RELATED WORK

Previous work on the topic of hair aging is divided into contributions on face aging and hair rendering.

Face Aging. The main goal of face aging is to render a face that looks either biologically younger or older than the original subject while still trying to preserve the person's identity. A recent survey by Grimmer et al. [2021] shows the many advances face aging in 2D has achieved. Although with impressive results [Alaluf et al. 2021], distinctive hair aging features such as hair graying and receding hairline are missing.

In 3D, previous research has addressed specific aspects, mostly skin changes, such as wrinkles [Li and Kry 2014; Nagano et al. 2015], dark spots [Barros and Walter 2017], and changes that occur in the skin's optical reflection properties as it ages [Iglesias-Guitian et al. 2015]. Some graphics engines allow hair graying in human models [Epic Games 2022]. The results look like a uniform random distribution of white hairs according to a gray amount percentage.

There is only one known hair graying model [Volkmann and Walter 2020] in computer graphics, which describes a simple aging system for male hair. Their method simulates the evolution of graying starting from the temporal region and spreading to the rest of the hair scalp at a later point of the process. They used manually segmented textures to separate the different scalp regions to control this effect. Due to a rough segmentation, there are visible seams along the many scalp regions as the aging advances. Their work is also limited to males and does not generalize to different hairstyles, such as long hair.

Hair Rendering. Hair rendering has achieved increasing levels of visual fidelity. These heightened realism levels are partly due to a better understanding and more complex modeling of hair structure and its interaction with light [Marschner et al. 2003]. This is a well-established topic, and many techniques focus on approximations to the light scattering phenomenon [Yuksel and Keyser 2008; Zinke et al. 2008]. d'Eon et al. [2011] presented a biology-inspired hair reflectance model. In their work, hair absorption is caused by the two types of natural pigments, *eumelanin* and *pheomelanin*. Based on the work of d'Eon, Chiang et al. [2016] produced a new hair reflectance model that is efficient enough for production *Path Tracing* while still having parameters that are easily controllable by artists. Together, the work of [d'Eon et al. 2011] and [Chiang et al. 2016] form the basis for biologically-inspired colored hair rendering in many graphics engines today such as Unreal Engine [Epic Games 2022] and Blender [Blender Foundation 2021].

Many approaches use deep learning for the rendering task [Saito et al. 2018; Wei et al. 2018; Yang et al. 2019a; Zhou et al. 2018], with very surprising results. The work of Bao and Qi [Bao and Qi 2018] details image-based approaches as input to modeling and simulation. Regarding animation tasks, Wu and Yuksel [Wu and Yuksel 2016] present a real-time approach, while other works focus on the interaction of hair with external elements such as water [Lee et al. 2018]. There have also been several developments in image-based hair capturing [Chai et al. 2016; Hu et al. 2014], data-driven hair modeling [Xing et al. 2019; Yang et al. 2019b] and synthesis [Olszewski et al. 2020]. Finally, hair geometry is typically modeled as explicit hair strands [Yu et al. 2012; Yuksel and Tariq 2010], although there are also volumetric representations [Petrovic et al. 2005; Xing et al. 2012], and even hybrid models [Jansson et al. 2019]. For our purposes, we need explicit hair geometry, modeled as a collection of hair follicles defined on the head's surface. Despite all these advances, the current solutions have not addressed the problem we address in this paper, hair aging.

3 BIOLOGY OF HAIR AGING

This section presents key concepts on hair aging that support design decisions in our solution. From the appearance of wrinkles and dark spots on the face to changes in skin tone, the human body has several ways to convey the passage of time: hair color is one of them. Hair color is determined by the amount and nature of the produced melanin, which are polymers synthesized from tyrosine. There are five types of melanin, but only two responsible for hair pigmentation: *eumelanin*, with color ranging from brown to black; and *phaeomelanin*, with color ranging from pale yellow to red [Cao et al. 2021].

There are two main visual effects concerning hair: hair graying (HG) and hair thinning. The first, hair graying, is due to the decrease over time in melanin granules' amount, size, and density. With age, normal color hair, gray, and white hairs co-exist [Tobin 2008], although there is no data on the incidence of each type as age advances. Fully white heads are not very common, since white hairs reach a plateau around 70-90% at 100 years old [Rosenberg et al. 2021].

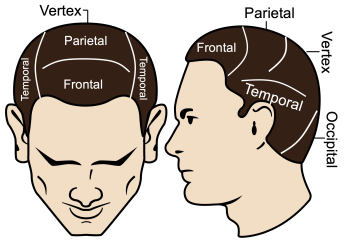

Fig. 2. Regions of the hair scalp. Adapted from [Marieb 2019].

Despite an ongoing investigation for decades, there is no universally accepted model for HG [O'Sullivan et al. 2021]. For our purpose of biologically-inspired simulation, we need to know the dynamics of gray spreading on the head since HG affects different regions of the hair scalp at different times across an individual's

lifespan. The scalp regions vary slightly among individuals and are named after bone structures illustrated in Fig. 2: *frontal*, *parietal*, *temporal*, *vertex*, and *occipital*. The vertex is not bone-related, and it is the area delimited by the parietal, temporal, and occipital areas.

From an extensive population study of 4,192 males and females aged between 45 and 65 years old from all over the world, Panhard et al. [2012] showed that in men, the temporal region has an incidence of 75% of gray hairs, compared to 67% on the vertex and 58% on the occipital area. The temporal region is the earliest to be affected, spreading to the vertex and then to the rest of the head [Tobin 2008]. For women, the onset area of gray seems to be either the parietal region [Acer et al. 2020] or the frontal area [Jo et al. 2012]. As in men, the occipital area was also the least affected.

The second visual effect is *hair thinning*, the decrease in hair diameter due to aging, around 40% to 70% [Fernandez-Flores et al. 2019]. Thinning usually starts after 50 years of age. The visual result of hair thinning is akin to hair loss and appears in the whole head, as illustrated in Fig. 7.

4 HAIR AGING MODEL

Our hair aging model has two main parts: hair graying and hair thinning. For HG, we introduce a spatial-aware aging model that simulates graying at different rates on the scalp, according to the region the hair belongs to. Our model extends recent work in biology that addressed the general graying process in hairs. Rosenberg et al. [2021], in a multinational team of researchers, developed a new method for digitizing hair shafts, allowing for a closer view of graying transitions across individual hair strands. Their main focus was on stress-related gray aging and discovering that the graying process is reversible in healthy hairs. Their main contribution is the *Aging Factor* (AF) for each hair. As the *AF* crosses a threshold, the follicle loses its capacity to produce melanin, turning white. This behavior is modeled by a linear mixed model, supporting both fixed and random effects to account for the stochastic nature of hair graying. For hair i and age a, the aging factor is given as [Rosenberg et al. 2021]:

$$AF_{i,a} = |b_{0,i}| + a(|b_{1,i}| + \beta_1) + AS_a(|b_{2,i}| + \beta_2) + e_i \quad (1)$$

where $b_{0,i}$ is the initial aging factor, β_1 is the aging factor rate, and β_2 describes how sensitive is the aging factor to stressful events. The variables $b_{1,i}$ and $b_{2,i}$ add random effects to, respectively, the *AF* rate and the sensitivity to stress for hair i. AS_a stands for the cumulative stress at a given age a and e_i accounts for measurement errors. The random effects $b_{0,i}$, $b_{1,i}$ and $b_{2,i}$ follow a multivariate Gaussian distribution. Rosenberg et al. [2021] defined default parameter values that describe the graying process for an average grayer, as well as for subjects who are affected by graying in an earlier or later stage of life, displayed in Table 1.

The idea of the *AF* is the first to quantitatively model hair graying, being a key contribution in the field of Biology, but uniformly subjecting all hairs in the head to the same graying mechanism. They did not address the different rates of graying across scalp regions, such as the early graying of the temporal area and the late graying of the occiput. Hence, we propose a spatially-aware model

Table 1. Default parameters for early, average and late grayers. For all distributions mean = 0, σ_0 and σ_1 are standard deviations for, respectively, b_0 and b_1. Source: Rosenberg et al. [2021].

Parameter	*Early*	*Average*	*Late*
β_1	16	16	16
σ_0	10	10	10
σ_1	25	13	8
Threshold	1920	1920	1920

that extends the *AF* definition for ***r* different distributions**, based on the scalp regions, as follows:

$$AF_{i,r,a} = |b_{0,i}| + a(|b_{1,i,r}| + \beta_1) \quad (2)$$

Since our work focuses on the hair simulation itself and not on external factors such as stress, which is left as future work, and the error term is negligible, we can remove those terms, and add the dependency on r different regions. Also, there is no correlation between the random variables $b_{0,i}$ and $b_{1,i}$ in the aging simulation from Rosenberg et al. [2021], and therefore, we will be using univariate normal distributions for each effect. Besides, their hair aging model is only concerned with fully pigmented and white hairs, and does not account for gray hairs. Our system incorporates this possibility by allowing the user to define the relative proportion of hairs that become either white or gray after crossing the threshold. In section 5.3 we explain how.

Hair thinning is a simpler effect to model compared to HG. Its decreasing effect on the hair shaft diameter is uniform in all hairs. Therefore, we model hair thinning as a linear decrease proportional to the current age a as:

$$ht_a = t(a - a_i)/(a_f - a_i) \quad (3)$$

where ht is the decrease amount in the $[0, t]$ interval, a_i, and a_f are respectively the initial and final ages for applying the effect, and t is the final desired amount of thinning.

5 METHODOLOGY

Our method has two parts: preprocessing and visual simulation. In preprocessing, we first segment the 3D character's head into the five regions: temporal (we count both temporal sides as one), frontal, parietal, occipital, and the vertex. Next, we compute the controlling parameters of hair aging (b_0,b_1) that will be used for each hair follicle in our real-time simulation. We save these values into textures that are sampled to control the rendering of our hair aging simulation. Fig. 3 shows an overview of our methodology.

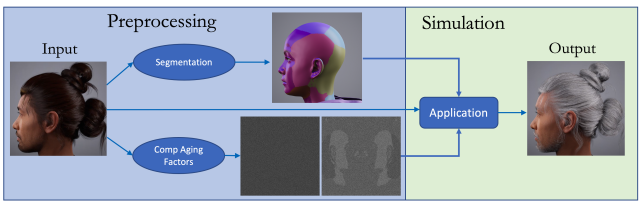

Fig. 3. Overview of our methodology.

5.1 Head Segmentation

Our insight into an automatic head segmentation according to the head's bone structure is that the normal vectors have distinct directions among head areas (Fig. 4(b)). We use clustering techniques to group normal vectors based on their orientation, thus defining regions by vectors similarity. Fig. 4 illustrates the method.

The scalp regions are labeled after the underlying skull bone structures, except for the vertex, which is the region delimited by the parietal, temporal, and occipital areas. The exact boundaries of these regions are individual to each person. In fact, an exact division is not strictly necessary since rendered hair diffuses the effect over the boundaries.

Our input for the clustering task is a modified version of the normal map of the model's head (Fig. 4(a)), where each texel represents the XYZ normal direction. The modified normal map has both sides symmetrical since the head is symmetric about the sagittal plane (the plane that cuts the body into left and right halves). We can apply k-means clustering only on half of the map and mirror the result to the other half with this modification. As the clustering happens in the same image space, our segmentation masks will inherently be textures wrapped around the model's head.

Although we were only concerned with five areas, we set K to eight. Our input image also contained data from the face, part of the neck, and parts that do not belong to any head part. These are surfaces with different orientations, and therefore we need to consider them when clustering. In Fig. 4(d), the final mapping segments the desired regions according to the anatomical areas of the head. Also, this process is consistent for all human head models we tested, regardless of gender or head shape variations.

5.2 Computing the Aging Factors

Here we present how we precompute the information needed to simulate graying in real-time. The defining mechanism for graying each hair is the Aging Factor (*AF*) given by Eq. 2. In summary, we need the values for β_1, b_0, and b_1 for each hair strand at a specific location on the scalp. To properly simulate graying at different rates in specific head parts, we need a way to accelerate or postpone the graying on a determined region. Of the three available values in Eq. 2 (β_1, b_0 and b_1), b_1 provides a more significant change in the total *AF*, as follows: β_1 is a fixed value for all hairs, and b_0 is simply added to the total *AF*, while b_1 is multiplied by the current year in the simulation. Therefore, we will use different values for the standard deviation (SD) of b_1 to accelerate or postpone the graying on a determined region r of the hair scalp.

There is no available data comparing the specific rates of graying on different hair zones throughout a person's lifespan, but we know the overall or global graying. Thus, our approach to finding appropriate SDs for b_1 is to use local rates of graying that are consistent with the global graying given by the computational model of Rosenberg et al. [2021]. As long as the overall number of white hairs on the scalp is consistent with the global graying, the percentage of gray hairs in each region can differ. This is a gender-dependent issue once the order of graying affects male and female subjects differently.

Table 2. Values of b_1 standard deviations.

Head Region	Male σ_1	Female σ_1
Temporal	16	13
Vertex	14	13
Parietal/frontal	13	16
Occipital	11	11
Facial hair	13	13

To compute the SDs for b_1 in each hair region while still conforming with the global rate of graying, we use a guided empirical approach. From the default values defined in Table 1, we know an upper and lower bound for b_1 SDs, given by the early and late grayers. We also know the number of hairs in each area and the default values for b_0 and β_1, defined in the same table. Therefore, we tested a few different possibilities of distributions for b_1 in each region. Each possibility was validated against the global rate of graying.

In Table 2 we present the defined SDs for males and females. We explain below the logic for males, although the same applies to females. The reasoning behind these values is that 13 is the same σ_1 used by Rosenberg et al. [2021] to simulate the hair aging of an average grayer. Therefore, if we establish that men's parietal and frontal regions age at an average speed – they are affected later than the temples and vertex, but before the occipital region – we can define these regions as having the average $\sigma_1 = 13$. Since the temples are the first area to age, they require the highest deviation value, followed by the vertex region. The occipital area is the last region to gray in both men and women, and therefore, it must have the lowest SD value. As seen in Fig. 5 for males, we were able to reach partial distributions that together are close to the original global rate of graying while still allowing for different rates in each region.

For facial hair, we also set $\sigma_1 = 13$, as this region is, on average, affected at a later time than the temples and vertex according to Tobin [2008]. For b_0, which does not vary along the hair scalp, we can sample from a distribution with $\sigma_0 = 10$. For b_1, we use the binary masks from the segmentation stage to decide, for each texel, which distribution to sample from. Once we have the values of b_0 and b_1 precomputed, they are stored in 8-bit textures with 2048^2 resolution to avoid aliasing.

5.3 Visual Simulation

The visual simulation of hair aging is performed in real-time. We implemented our method inside Unreal Engine (UE) 5 [Epic Games 2022], although any modern graphics engine with similar features could be used. The human models are from Metahumans [Epic Games 2021]. The inputs required for the simulation are the 3D model of the head together with hair and the texture maps for b_0 and b_1 previously generated. We also need the target age for the subject or an age interval. In the latter case, if the final age is smaller than the initial age, a *deaging* effect is simulated. In Algorithm 1 we present the visual simulation algorithm.

The inputs for the simulation are the amount t of thinning desired, β_1 and the threshold from [Rosenberg et al. 2021]. We start with the main loop for the age interval, followed by a second loop over all

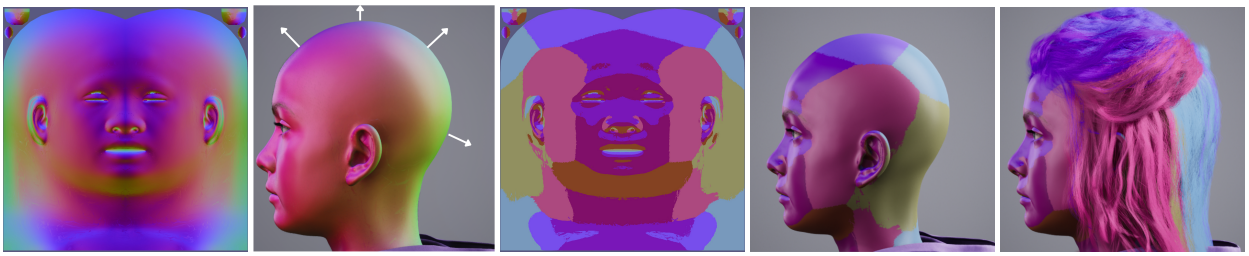

(a) Modified Normal map (b) Normal vectors (c) Segmentation mask (d) Mask applied to head (e) Mask used in hair

Fig. 4. (a) represents the modified normal map; (b) is an illustration showing average normal vectors; (c) is the final output of K-Means; (d) the texture applied on the model's face; (e) shows the segmentation of the hairs according to the location of their roots on the surface of the head.

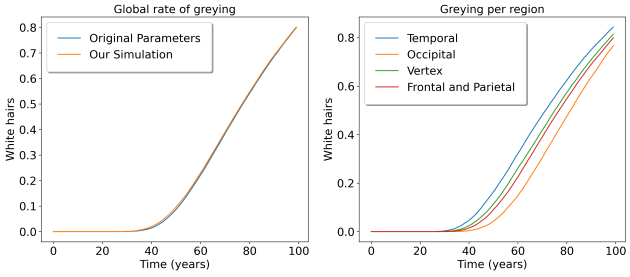

Fig. 5. On the left is a comparison between a simulation run with the original parameters, in blue, and one using the values defined for specific hair regions, in orange. There is no significant difference between the two models. The right image shows the aging disparity in each region for a male model, as the temples, vertex, frontal/parietal, and occipital regions reach 50% of gray hairs at 72, 76, 78, and 82 years of age.

(a) gray: 0% (b) gray: 50% (c) gray: 100%

Fig. 6. Effect of having white hairs or not. In (a), only white hairs. All the hairs that have crossed the threshold have their melanin amounts reduced to a minimum value, resulting in more visible seams between hair regions with different aging rates. In (b) an equal mixture of gray and white hairs, allowing the discontinuities to blend while still having hairs with little melanin. In (c), there are no white hairs, and therefore the result lacks the tonal range seen in real-life grayers.

hairs. Before applying graying, we check if thinning will be applied (line 5). To compute the AFs, we first need the region where the hair resides (line 8) and the values for $b_{0,i,r}$ and $b_{1,i,r}$ sampled from the precomputed textures (line 9). After computing AF (line 10), we check if this hair has reached the threshold: if not, the loop on the hairs moves on to the next hair; if yes, we perform an implicit loop over the length of the hair strand to render each section of

Algorithm 1 Visual Simulation

```
1:  Inputs: t, β1 and threshold from Table 1
2:  for a = a_i, ..., a_f do                          ▷ Age Interval
3:      Compute ht(a) (Eq. 3)                         ▷ t used here
4:      for i = 1, 2, ..., N do                       ▷ For all hairs
5:          if Thinning then
6:              Apply ht on hair i
7:          end if
8:          r defined from (u, v) coordinates         ▷ Which region?
9:          Sample b_{0,i,r} and b_{1,i,r} from textures
10:         Compute AF_{i,r,a} (Eq. 2)
11:         if AF_{i,r,a} > threshold then
12:             if Decrease(i) then
13:                 if gray then                      ▷ is it gray or white?
14:                     DecreaseMelanin(i)
15:                     Desaturate(i)
16:                     Render hair i gray
17:                 else
18:                     DecreaseMelanin(i)
19:                     Render hair i white
20:                 end if
21:             end if
22:         end if
23:     end for
24: end for
```

an i-th hair according to the *Decrease* condition (lines 12-21). This condition indicates whether the current point on the strand should have its melanin amount decreased. We check if enough time has passed for the unpigmented part to reach the length of the current point in the strand, starting when the hair crosses the threshold (line 12). We describe the condition as:

$$Decrease = \begin{cases} yes, & \text{if } HL - TPT * YG < 0 \\ no, & \text{otherwise} \end{cases}$$

where *HairLength (HL)* is defined in centimeters as the current length of the hair shaft at the shading point, and *Yearly Growth (YG)* is $12cm/year$ [LeBeau et al. 2011]. *TimePastThreshold (TPT)* is the elapsed time in years since a hair's AF crossed the Threshold. It is calculated as follows, for an i-th hair:

$$TPT_i = \frac{AF_i - Threshold}{\beta_1 + b_{1,i}} \tag{4}$$

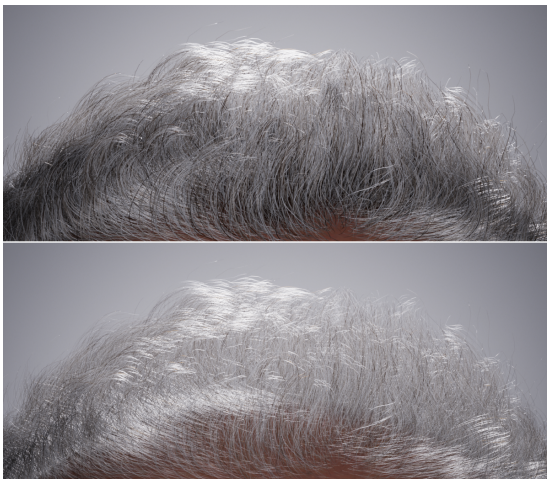

Fig. 7. Example of hair thinning on a digital model. The hair diameter was reduced by 60% from the hairs in the top figure to the bottom figure.

Our system allows both gray and white hairs (line 13) in proportions controlled by the user. There is no data regarding this percentage in the literature. We found that a percentage of 50% yielded the best results through visual comparisons with real-life subjects. Fig. 6 shows a comparison of different proportions of gray-to-white hairs. Finally, we have to decrease the amount of melanin at the shading point, either gray or white. UE's implementation of melanin in the hair shader uses only a variable called *Melanin* to account for both eumelanin and pheomelanin, and a *Redness* value representing the ratio between them. Therefore, we will be referring to UE's *Melanin* when discussing the decrease of melanin, as the ratio between the two types of melanin does not change after the decrease. Even with a lower amount of melanin for gray hairs, the hair is still saturated. Thus, we transform the RGB color into the corresponding grayscale (Desaturation – line 15).

6 RESULTS

This section discusses the results obtained with our method implemented using Unreal Engine 5 (UE5) and Metahumans. We performed our tests on an Intel i7 3770k @ 3.5 GHz paired with an NVIDIA RTX 2070 SUPER on Windows 10, averaging 45 FPS at 1920x1080, at *Cinematic Quality* settings in UE5. Preprocessing is approximately 5 minutes, while segmentation takes around 45 seconds. Our results are better appreciated when animated over time. Please check the companion video for more results. The teaser figure shows the generality of our method over different hairstyles and gender. We show the graying of a white male, a red-hair female, and a male with black hair and beard.

We can apply hair thinning independently of the hair graying effect. Fig. 7 shows a close-up of hair thinning on a digital character. The use of hair thinning increases the overall visual realism of the results, particularly at older ages, when the effect is more noticeable. Unless otherwise stated, all our results used hair thinning with a default linear reduction of 60% of hair diameter over the age interval.

In Fig. 8 we compare our work with the results of [Volkmann and Walter 2020], the only reported system for hair aging. Volkmann's work presented their results with real subjects for a given age range, not a specific age. Therefore we were not able to make direct comparisons. In general, our results present smoother transitions and a more natural overall graying since we model better the hair to hair heterogeneity as in real greying [Rosenberg et al. 2021], with neighboring hairs at different stages.

We also compare our results with the Metahuman graying effect in Fig. 9. Their system allows the simulation of graying through a *WhiteAmount* slider that interpolates between 100% pepper – fully pigmented, to 100% salt – white hairs. The effect is applied overall in all hairs with some random distribution. The method does not incorporate the notion of time and can only be manually controlled by artists. For the results in the figure, we tweak the salt-and-pepper values to render hair at a similar stage of graying. We can see, particularly at older ages, that MetaHuman's *WhiteAmount* only changes the overall number of gray hairs on the hair scalp, with a result more uniform than expected for a man.

In Fig. 10 we compare the dynamics of graying for men and women. While the first to gray in men is the temporal region, the frontal and parietal regions are the first to gray for women. Fig. 11 shows a female result with blond hair and an older human, where the graying looks more natural. Also, in Fig. 12, we show an example of hair greying for a woman with long black hair. The effect of thinning is clearly noticeable at the frontal region, where hair appears less voluminous as the simulation advances. Finally, in Fig. 13, we compare our results to the hair graying 6-stage classification system suggested by Pośpiech et al. [2020], where in general, our simulation follows the pattern suggested in each category. There are some differences in categories 5 and 6. For category 5, we believe it could be a matter of lighting conditions and hairstyling. While the real-life subject has short straight hair, our 3D character has a more voluminous curly hair, which results in more self-shadowing. In category 6, we believe that photodegradation could cause the yellowing of the subject's hair [Richena et al. 2014], a condition we do not yet model.

7 CONCLUSIONS

We presented a real-time solution for the simulation of the hair aging phenomenon. The system is biologically inspired and supports facial hair, genders, and varied hairstyles. As our model does not require artistic input, we expect the average user can use it to age 3D characters in a convincing fashion. Besides the expected applications in games or the movie industry, we believe our work can assist biological research, providing a better visual understanding of the hair aging process for hypothesis testing.

We developed our system based on data for three different graying speeds: early, average, and late. However, graying could affect someone later than our early grayer setting but earlier than the average grayer. In this case, the hair could have a different appearance than the one provided by our model at the same age. Also, our model does not account for the ethnic origin of our character, a property that could influence the rate of graying, as presented by Panhard et al. [2012].

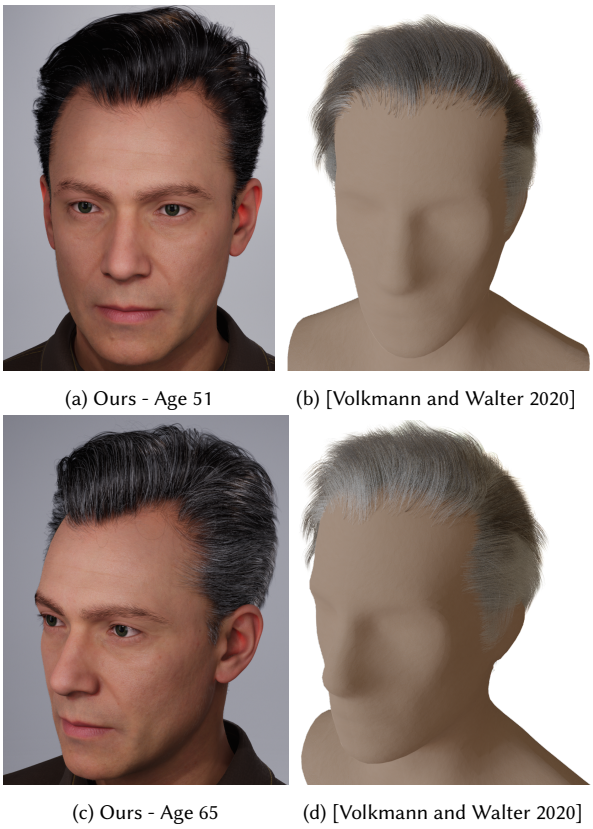

(a) Ours - Age 51 (b) [Volkmann and Walter 2020]

(c) Ours - Age 65 (d) [Volkmann and Walter 2020]

Fig. 8. Comparison with prior work. Our model can simulate the early graying of the temporal area, which is also done by the method of Volkmann and Walter [2020]. However, the model in (b) has a visible seam on the temples at the point where the gray hairs end. In contrast, our model blends the different areas by having a few parietal and frontal hairs graying earlier than average. There is a clear discontinuity in (d) among different regions of the hair scalp.

Finally, we address some limitations of our work. The material properties of hair change with time, which we represent through hair thinning in our model. However, it is known that a hair shaft also becomes dry and fragile with age [Fernandez-Flores et al. 2019]. It is not clear how these other aging effects translate visually. Furthermore, our system only models the aging of healthy hair. Genetic hair conditions that are usually accentuated with age, such as female and male pattern hair loss - which includes receding hairlines - are not currently addressed by our work. Hence, changes in hair volume in our results are more subtle, although still present in the form of hair thinning.

In future work, we plan to develop a more general, robust framework that accounts for the geographical origin of our subject. Besides, we hope to incorporate external factors that can affect hair aging, such as stress and the effect of the associated graying reversal. Although Rosenberg et al. [2021] presented how to model the effects of stress, the computational cost of simulating their approach would be too expensive in our current system. As they use a multivariate distribution to model hair aging, and the parameter maps in our system have a resolution of 2048^2, we would be required to draw 4M samples from this distribution for each map. This would result in a significant increase in computation time compared to drawing the same 4M samples from a univariate distribution, as used in our method.

ACKNOWLEDGMENTS

We thank Prof. Manuel de Oliveira for the many helpful suggestions that helped improve our initial submission and the final version of our work. This study was financed in part by the Coordenação de Aperfeiçoamento de Pessoal de Nível Superior - Brasil (CAPES) - Finance Code 001. We also thank Poatek for travel funding.

REFERENCES

Ersoy Acer et al. 2020. Clinical and epidemiological characteristics and associated factors of hair graying: a population-based, cross-sectional study in Turkey. *Anais Brasileiros De Dermatologia* 95, 4 (2020), 439–446. https://doi.org/10.1016/j.abd.2020.03.002

Yuval Alaluf, Or Patashnik, and Daniel Cohen-Or. 2021. Only a matter of style: Age transformation using a style-based regression model. *ACM Transactions on Graphics* 40, 4 (2021), 1–12.

Yongtang Bao and Yue Qi. 2018. A survey of image-based techniques for hair modeling. *IEEE Access* 6 (2018), 18670–18684.

R. S. Barros and M. Walter. 2017. Synthesis of Human Skin Pigmentation Disorders. *Computer Graphics Forum* 36, 1 (2017), 330–344.

Blender Foundation. 2021. *Unity 2021.* https://www.blender.org

Wei Cao et al. 2021. Unraveling the Structure and Function of Melanin through Synthesis. *Journal of the American Chemical Society* 143, 7 (2021), 2622–2637.

Menglei Chai, Tianjia Shao, Hongzhi Wu, Yanlin Weng, and Kun Zhou. 2016. AutoHair: Fully Automatic Hair Modeling from a Single Image. *ACM Transactions on Graphics* 35, 4 (2016). https://doi.org/10.1145/2897824.2925961

M J Chiang, B Bitterli, C Tappan, and B Burley. 2016. A Practical and Controllable Hair and Fur Model for Production Path Tracing. *Computer Graphics Forum* 35, 2 (2016), 275–283.

Eugene d'Eon, Guillaume Francois, Martin Hill, Joe Letteri, and Jean-Marie Aubry. 2011. An Energy-Conserving Hair Reflectance Model. *Computer Graphics Forum* 30, 4 (2011), 1181–1187.

Epic Games. 2021. *MetaHuman Creator.* https://metahuman.unrealengine.com/

Epic Games. 2022. *Unreal Engine 5.* https://www.unrealengine.com

Angel Fernandez-Flores, Marcela Saeb-Lima, and David S. Cassarino. 2019. Histopathology of aging of the hair follicle. *Journal of Cutaneous Pathology* 46, 7 (2019), 508–519. https://doi.org/10.1111/cup.13467

Y. Gitlina et al. 2020. Practical Measurement and Reconstruction of Spectral Skin Reflectance. *Computer Graphics Forum* 39, 4 (2020), 75–89.

Marcel Grimmer, Raghavendra Ramachandra, and Christoph Busch. 2021. Deep face age progression: A survey. *IEEE Access* 9 (2021), 83376–83393.

Liwen Hu, Chongyang Ma, Linjie Luo, Li-Yi Wei, and Hao Li. 2014. Capturing Braided Hairstyles. *ACM Transactions on Graphics* 33, 6 (2014), 225:1–225:9.

J A Iglesias-Guitian, C Aliaga, A Jarabo, and D Gutierrez. 2015. A biophysically-based model of the optical properties of skin aging. In *Computer Graphics Forum*, Vol. 34. 45–55.

Erik Sven Vasconcelos Jansson, Matthäus G. Chajdas, Jason Lacroix, and Ingemar Ragnemalm. 2019. Real-Time Hybrid Hair Rendering. In *Eurographics Symposium on Rendering - DL-only and Industry Track*, Tamy Boubekeur and Pradeep Sen (Eds.). The Eurographics Association. https://doi.org/10.2312/sr.20191215

Seong Jin Jo et al. 2012. Hair graying pattern depends on gender, onset age and smoking habits. *Acta dermato-venereologica* 92, 2 (2012), 160–161.

Hyeong-Seok Ko, Kwang-Jin Choi, Min Gyu Choi, Seyoon Tak, Byoungwon Choe, and Oh-Young Song. 2003. Research Problems for Creating Digital Actors. In *Eurographics (State of the Art Reports).*

Marc A. LeBeau, Madeline A. Montgomery, and Jason D. Brewer. 2011. The role of variations in growth rate and sample collection on interpreting results of segmental analyses of hair. *Forensic Science International* 210, 1 (2011), 110–116.

M Lee, D Hyde, M Bao, and R Fedkiw. 2018. A skinned tetrahedral mesh for hair animation and hair-water interaction. *IEEE TVCG* 25, 3 (2018), 1449–1459.

Pengbo Li and Paul G Kry. 2014. Multi-layer skin simulation with adaptive constraints. In *Proceedings of the Seventh International Conference on Motion in Games.* 171–176.

Stephen Lombardi, Tomas Simon, Gabriel Schwartz, Michael Zollhoefer, Yaser Sheikh, and Jason Saragih. 2021. Mixture of Volumetric Primitives for Efficient Neural Rendering. *ACM Transactions on Graphics* 40, 4 (2021).

Nadia Magnenat-Thalmann. 2004. Photorealistic hair modeling, animation, and rendering. In *ACM SIGGRAPH 2004 Course Notes.*

(a) Ours - Age 51 (b) Ours - Age 58 (c) Ours - Age 65 (d) Ours - Age 74 (e) Ours - Age 100

(f) MH *WhiteAmount*: 0.04 (g) MH *WhiteAmount*: 0.1 (h) MH *WhiteAmount*: 0.3 (i) MH *WhiteAmount*: 0.6 (j) MH *WhiteAmount*: 0.9

Fig. 9. Comparison of our aging system with the salt-and-pepper alternative from MetaHumans. Our sequence shows the progression of graying on the head regions as expected, starting in the temporal area and finishing in the occipital area. In contrast, increasing the MetaHuman's (MH) *WhiteAmount* only changes the overall number of gray hairs without following the hair aging pattern for a man. Also, we can notice the effect of hair thinning at the end of our simulation in (e), which is primarily visible around the vertex and occipital zones.

(a) Man - Age 58 (b) Man - Age 65 (c) Man - Age 74

(d) Woman - Age 58 (e) Woman - Age 65 (f) Woman - Age 74

Fig. 10. Male vs Female hair graying.

Fig. 11. Hair aging applied to a female with blond hair. Hair thinning is visible at the whorl in the vertex region.

Elaine N. Marieb. 2019. *Essentials of Human Anatomy & Physiology, Global Edition.* Pearson.

Stephen R Marschner et al. 2003. Light scattering from human hair fibers. *ACM Transactions on Graphics* 22, 3 (2003), 780–791.

Koki Nagano et al. 2015. Skin microstructure deformation with displacement map convolution. *ACM Transactions on Graphics* 34, 4 (2015), 109–1.

Kyle Olszewski, Duygu Ceylan, Jun Xing, Jose Echevarria, Zhili Chen, Weikai Chen, and Hao Li. 2020. Intuitive, Interactive Beard and Hair Synthesis With Generative Models. In *Proceedings of the IEEE/CVF Conference on Computer Vision and Pattern Recognition (CVPR).*

James DB O'Sullivan, Carina Nicu, Martin Picard, Jérémy Chéret, Barbara Bedogni, Desmond J Tobin, and Ralf Paus. 2021. The biology of human hair greying. *Biological Reviews* 96, 1 (2021), 107–128.

S. Panhard et al. 2012. Greying of the human hair: a worldwide survey, revisiting the '50' rule of thumb. *British Journal of Dermatology* 167, 4 (2012), 865–873.

Lena Petrovic, Mark Henne, and John Anderson. 2005. Volumetric methods for simulation and rendering of hair. *Pixar Animation Studios* 2, 4 (2005).

Ewelina Pośpiech et al. 2020. Exploring the possibility of predicting human head hair greying from DNA using whole-exome and targeted NGS data. *BMC genomics* 21, 1 (2020), 1–18.

(a) Category 1 (b) Category 2 (c) Category 3

(d) Category 4 (e) Category 5 (f) Category 6

Fig. 13. Comparison between the six-stage classification system suggested by [Pośpiech et al. 2020] in the upper row and our simulations, in the bottom row. The six stages are defined as (a) no greying, (b) predominantly no greying, with low number of single grey hairs, (c) higher number of single grey hair (all over head), (d) significant greying with patches of grey hair, (e) predominantly greying, (f) totally white hair.

Fig. 12. Hair aging applied to a female with long black hair. Greying happens first at the top of the head, later progressing to the occipital region.

M. Richena, M. Silveira, C.A. Rezende, and I. Joekes. 2014. Yellowing and bleaching of grey hair caused by photo and thermal degradation. *Journal of Photochemistry and Photobiology B: Biology* 138 (2014), 172–181.

Ayelet M Rosenberg et al. 2021. Quantitative mapping of human hair greying and reversal in relation to life stress. *eLife* 10 (June 2021), e67437.

G Ryder and AM Day. 2005. Survey of Techniques for Rendering Real-Time Virtual Humans. *Computer Graphics Forum* 24, 2 (2005), 203–215.

Shunsuke Saito, Liwen Hu, Chongyang Ma, Hikaru Ibayashi, Linjie Luo, and Hao Li. 2018. 3D hair synthesis using volumetric variational autoencoders. *ACM Transactions on Graphics* 37, 6 (2018), 1–12.

D. J. Tobin. 2008. Human hair pigmentation – biological aspects. *International Journal of Cosmetic Science* 30, 4 (2008), 233–257.

Diego V. Volkmann and Marcelo Walter. 2020. A Practical Male Hair Aging Model. In *Eurographics 2020 - Short Papers*, Alexander Wilkie and Francesco Banterle (Eds.). https://doi.org/10.2312/egs.20201017

Lingyu Wei, Liwen Hu, Vladimir Kim, Ersin Yumer, and Hao Li. 2018. Real-time hair rendering using sequential adversarial networks. In *Proceedings of the European Conference on Computer Vision (ECCV)*. 99–116.

Kui Wu and Cem Yuksel. 2016. Real-time hair mesh simulation. In *Proceedings of the 20th ACM SIGGRAPH Symposium on Interactive 3D Graphics and Games*. 59–64.

Jun Xing, Koki Nagano, Weikai Chen, Haotian Xu, Li-yi Wei, Yajie Zhao, Jingwan Lu, Byungmoon Kim, and Hao Li. 2019. HairBrush for Immersive Data-Driven Hair Modeling. In *Proceedings of the 32nd Annual ACM Symposium on User Interface Software and Technology (UIST '19)*. 263–279. https://doi.org/10.1145/3332165.3347876

Xiaoxiong Xing et al. 2012. Real-Time Rendering of Animated Hair under Dynamic, Low-Frequency Environmental Lighting. In *Proc. 11th SIGGRAPH VRCAI*. 43–46.

Lingchen Yang, Zefeng Shi, Youyi Zheng, and Kun Zhou. 2019a. Dynamic hair modeling from monocular videos using deep neural networks. *ACM Transactions on Graphics* 38, 6 (2019), 1–12.

Lingchen Yang, Zefeng Shi, Youyi Zheng, and Kun Zhou. 2019b. Dynamic Hair Modeling from Monocular Videos Using Deep Neural Networks. *ACM Trans. Graph.* 38, 6, Article 235 (nov 2019), 12 pages.

Xuan Yu et al. 2012. A Framework for Rendering Complex Scattering Effects on Hair. In *Proceedings of the ACM SIGGRAPH I3D*. 111–118.

Cem Yuksel and John Keyser. 2008. Deep Opacity Maps. *Computer Graphics Forum* 27, 2 (2008), 675–680.

Cem Yuksel and Sarah Tariq. 2010. Advanced Techniques in Real-Time Hair Rendering and Simulation. In *ACM SIGGRAPH 2010 Courses (SIGGRAPH '10)*.

Yi Zhou et al. 2018. Hairnet: Single-view hair reconstruction using convolutional neural networks. In *Proceedings of ECCCV*. 235–251.

Arno Zinke, Cem Yuksel, Andreas Weber, and John Keyser. 2008. Dual Scattering Approximation for Fast Multiple Scattering in Hair. *ACM Transactions on Graphics* 27, 3 (2008), 1–10.